Supplementary information for Push-Pull Amino-substituted Heteroleptic Iron *N*-Heterocyclic Carbene Photosensitizers in Dye-Sensitized Solar Cells: Optimization and Characteristics

Samuel Persson[a†], Iacopo Benesperi[b,c], Yogesh Goriya[a], Dnyaneshwar Kand[a], Suresh Rayavarapu[a], Timo Keller[b], Marina Freitag[b]*, Kenneth Wärnmark[a]*

[a] Centre for Analysis and Synthesis, Department of Chemistry, Lund University, Box 124, SE-22100 Lund, Sweden.

[b] School of Natural and Environmental Science, Bedson Building, Newcastle University, NE1 7RU, Newcastle upon Tyne, UK.

[c] Department of Chemistry, NIS Interdepartmental Centre and INSTM Reference Centre, University of Turin, Via Quarello 15/A, 10135 Torino (TO), Italy

*Corresponding author.

Synthesis

Gereral. All commercial reagents and solvents were used as received, unless otherwise stated. 1,1'-(pyridine-2,6-diyl)bis(3-methylimidazolium)) dibromide ([H_2(pbmi)]Br_2) was purchased from TCI and stored in desiccator. Hydrochloric acid (concd. aq.) was purchased from VWR. KO*t*-Bu (1 M solution in THF) was purchased in septa-fitted bottles from Sigma-Aldrich and stored in refrigerator. Ammonium hexafluorophosphate (NH_4PF_6) was purchased from Sigma-Aldrich and stored in desiccator. Anhydrous iron(II) bromide ($FeBr_2$) was purchased from Sigma-Aldrich and stored and weighed under argon in a glovebox. THF without stabilizer was dried over Na/benzophenone and subsequently distilled under N_2, and further dried over activated molecular sieves (3Å) before use. Dry DMF was collected from dry solvent dispenser (Innovative technology, PS-micro) and further dried over activated molecular sieves (3Å) before use. (1,1'-(4-Carboxypyridine-2,6-diyl)bis(3-methylimidazolium)) bis(hexafluorophosphate) ([H_2(cpbmi)]$(PF_6)_2$),[S1] (1,1'-(4-(Dimethylamino)pyridine-2,6-diyl)bis(3-methylimidazolium)) bis(hexafluorophosphate) ([H_2(dmapbmi)]$(PF_6)_2$),[S2] (1,1'-(4-Carboxypyridine-2,6-diyl)bis(3-methylimidazol-2-ylidene))(1,1'-(4-(di-*p*-tolylamino)pyridine-2,6-diyl)bis(3-methylimidazol-2-ylidene))iron(II) bis(hexafluorophosphate) ([Fe(cpbmi)(dtapbmi)]$(PF_6)_2$ (**2**)), and (1,1'-(4-(Di-*p*-anisylamino)pyridine-2,6-diyl)bis(3-methylimidazol-2-ylidene)) (1,1'-(4-carboxypyridine-2,6-diyl)bis(3-methylimidazol-2-ylidene))iron(II) bis(hexafluorophosphate) ([Fe(cpbmi)(daapbmi)]$(PF_6)_2$ (**3**)[S3] were prepared according to literature procedures. Reactions run at room temperature (rt) were in the range of 18-23 °C. Metal heating mantels were used to achieve required reaction temperatures. Reactions were carried out in oven-dried glassware capped with rubber septa, under a positive pressure of nitrogen. Flash column chromatography (⌀ x h) was carried out on silica gel (60 Å, 230-400 mesh, purchased from Merck) using reagent-grade eluents. Analytical thin-layer chromatography (TLC) was carried out on TLC Silica gel 60 F254 and visualized with a UV-lamp (254 nm/365 nm). ^{1}H NMR and ^{13}C NMR spectra were recorded at rt on a Bruker Avance II spectrometer at 400.1 MHz and 100.6 MHz, respectively. The spectra were recorded in CD_3CN and the residual solvent signal (1.94/118.26 ppm) were used as reference. Chemical shifts (δ) are expressed in parts per million (ppm) and coupling constants (J) are reported in Hertz (Hz). The following abbreviations are used to indicate apparent multiplicities: s, singlet; d, doublet; dd, doublet of doublets; dq, doublet of quartets; t, triplet; td, triplet of doublets, q, quartet, m, multiplet. Melting points were measured using a Stuart melting point apparatus SMP3 and were corrected against caffeine (mp 238 °C[S4]; used for **1**) or 4-methoxybenzoic acid (mp 184 °C[S4]; used for **4**). IR transmittance spectra were recorded on a Bruker-ALPHA II FT-IR Spectrometer and reported in cm^{-1} with the following abbreviations used to report relative signal strength: w, weak; m, medium; s, strong; vs, very strong; and br, broad. High resolution mass spectrometry was carried out using a Waters - XEVO-G2 QTOF spectrometer employing

electrospray ionization and run in positive mode. Elemental analyses were performed by A. Kolbe, Mikroanalytisches Laboratorium, Germany.

((1,1'-(4-Carboxypyridine-2,6-diyl)bis(3-methylimidazol-2-ylidene))(1,1'-(pyridine-2,6-diyl)bis(3-methylimidazol-2-ylidene))iron(II)) bis(hexafluorophosphate) ([Fe(cpbmi)(pbmi)](PF$_6$)$_2$ (1)). A mixture of 1,1'-(pyridine-2,6-diyl)bis(3-methylimidazolium) bis(hexafluorophosphate) (184.5 mg, 0.3473 mmol) and 1,1'-(4-carboxypyridine-2,6-diyl)bis(3-methylimidazolium) bis(hexafluorophosphate) (200.4 mg, 0.3484 mmol) was dried *in vacuo* at 80 °C for 4 d. The solid was allowed to cool to rt under N_2, suspended in dry DMF (7 mL) and cooled to 0 °C. To the mixture was KO*t*-Bu (THF, 1 M, 2.1 mL, 2.1 mmol) added dropwise to the suspension over 9 min, and stirred at 0 °C for 30 min. To the resulting red solution was a solution of anhydrous $FeBr_2$ (81 mg, 0.38 mmol) in dry DMF (2 mL) added dropwise at 0 °C, over 7 min. Upon complete addition, the reaction was stirred for 20 min and was then allowed to warm to rt and stirred at that temperature for 21 h. The reaction mixture was diluted with EtOAc (70 mL) and extracted with water (3 x 70 mL), at which point the aqueous phase became almost colorless. The combined red aqueous phases were acidified with HCl (aq., 6 M) to pH = 1. To the resulting aqueous solution was added NH_4PF_6 (1 g, 6 mmol), and the resulting aqueous solution was extracted with EtOAc (3 x 150 mL). The combined organic phases were reduced *in vacuo*. The crude product was further purified by acidic alumina gel chromatography (3.5 x 18 cm, MeCN/H_2O 1:0 → 5:1 → 3:1). The desired fractions were combined and MeCN was evaporated *in vacuo*. The resulting aqueous solution was acidified by HCl (aq., 5 M) to pH = 1 and to it was added NH_4PF_6 (780 mg, 4.8 mmol). The resulting precipitate was filtered off on a glass filter (#4) and carefully rinsed with a few drops of ice-cold water until the filtrate becomes slightly coloured, giving **([Fe(cpbmi)(pbmi)](PF$_6$)$_2$** (67 mg, 22 %) as a dark red solid. R_f = 0.27 (MeCN/H_2O/KNO_3 (saturated aq.) 20:8:1). Mp: 251 °C dec. ^{1}H NMR (400 MHz, CD_3CN) δ = 8.27 (s, 2H, cPy-*H*3), 8.23 (t, *J* = 8.2 Hz, 1H, nPy-*H*4), 8.15 (d, *J* = 2.2 Hz, 2H, cIm-*H*4), 8.00 (d, *J* = 2.2 Hz, 2H, nIm-*H*4), 7.76 (d, *J* = 8.2 Hz, 2H, nPy-*H*3), 7.02 (d, *J* = 2.2 Hz, 2H, cIm-*H*3), 6.98 (d, *J* = 2.2 Hz, 2H, nIm-*H*3), 2.53 (s, 6H, cIm-CH_3), 2.47 (s, 6H, nIm-CH_3) ppm. ^{13}C NMR (101 MHz, CD_3CN) δ = 200.41, 200.24, 165.13, 155.66, 154.54, 140.17, 139.33, 127.63, 127.58, 117.63, 117.43, 106.59, 105.38, 35.57, 35.40 ppm. IR $\tilde{\nu}_{max}$ = 3143 (w, br), 1722 (w, br), 1620 (w), 1580 (w), 1546 (w), 1484 (s), 1408 (w), 1347 (w), 1270 (s), 1240 (m), 1086 (w), 1023 (w), 839 (vs), 792 (w), 739 (w), 687 (m), 557 (s), 487 (w) cm^{-1}. HRMS: [M^{2+} + PF6] Exp: 723.1231; Found: 723.1239. Anal. Calcd for $C_{27}H_{26}F_{12}FeN_{10}O_2P_2 \cdot 1.55\ H_2O$: C 36.18, H 3.27, N 15.63. Found: C 36.17, H 3.26, N 15.63

(1,1'-(4-carboxypyridine-2,6-diyl)bis(3-methylimidazol-2-ylidene))(1,1'-(4-(Dimethylamino)pyridine-2,6-diyl)bis(3-methylimidazol-2-ylidene))iron(II) bis(hexafluorophosphate) ([Fe(cpbmi)(dmapbmi)](PF$_6$)$_2$ (4)). A mixture of (1,1'-(4-(Dimethylamino)pyridine-2,6-diyl)bis(3-methylimidazolium)) bis(hexafluorophosphate) (100 mg, 0.174 mmol) and (1,1'-(4-carboxypyridine-2,6-diyl)bis(3-methylimidazolium)) bis(hexafluorophosphate) (100 mg, 0.174 mmol) was dried overnight, in vacuum at 80 °C. The solid was allowed to cool to rt under N_2, suspended in dry THF (10 mL) and cooled to -78 °C. To the mixture was KO*t*-Bu (THF, 1 M, 1.2 mL, 1.2 mmol) added dropwise over 9 min, and stirred at -78 °C for 30 min. To the resulting amber solution was a solution of anhydrous $FeBr_2$ (86 mg, 0.40 mmol) in dry THF (18 mL) added dropwise at -78 °C, over 20 min. The resulting black solution was allowed to warm to rt and stirred at that temperature for 1 h. The reaction mixture was evaporated *in vacuo.* The residue was dissolved in water and passed through a glass filter (#3). The resulting filtrate was acidified with dilute HCl (aq.) to pH ≤ 1, and to the resulting solution was then added NH_4PF_6 (360 mg, 2.2 mmol). The resulting precipitate was collected on a glass filter (#4) and further purified by alumina gel chromatography (3.5 x 15 cm, MeCN/H_2O 5:1 → 3:1). The desired fractions were combined and the MeCN was evaporated *in vacuo*. To resulting aqueous solution was acidified with dilute HCl (aq.) to pH ≤ 1 and to it was added NH_4PF_6 (390 mg, 2.4 mmol). The resulting precipitate was collected on a glass filter (#4) and carefully rinsed with a few drops of ice-cold water until the filtrate becomes slightly coloured, giving **([Fe(cpbmi)(dmapbmi)](PF$_6$)$_2$** as a red solid (21 mg, 13 %). R_f = 0.30 (MeCN/H_2O/KNO_3 (saturated aq.) 25:8:1). Mp: 174 °C dec. ^{1}H NMR (400 MHz, CD_3CN) δ = 8.22 (s, 2H, cPy-*H*3), 8.14 (d, *J* = 2.2 Hz, 2H, cIm-*H*4), 7.93 (d, *J* = 2.2 Hz, 2H, ani-Im-*H*4), 7.04 (d, *J* = 2.2

Hz, 2H, cIm-*H*3), 7.01 (s, 2H, ani-Py-*H*3), 6.91 (d, *J* = 2.2 Hz, 2H, ani-Im-*H*3), 3.27 (s, 6H, N-C*H*3), 2.71 (s, 6H, cIm-C*H*3), 2.39 (s, 6H, ani-Im-C*H*3) ppm. ^{13}C NMR (101 MHz, CD_3CN) δ = 201.39, 201.33, 165.43, 159.12, 156.32, 153.29, 137.47, 127.34, 127.06, 117.38, 116.99, 104.72, 91.02, 40.87, 35.55, 35.49 ppm. IR $\tilde{\nu}_{max}$ = 3151 (w, br), 1722 (w), 1644 (s), 1573 (w), 1537 (m), 1484 (s), 1405 (w), 1345 (w), 1268 (s), 1235 (w), 1179 (w), 1084 (w), 940 (w), 839 (vs), 804 (w), 721 (w), 688 (s), 558 (w) cm^{-1}. HRMS: [M^{2+} + PF6] Exp: 766.1653; found: 766.1653. Anal. Calcd for $C_{29}H_{31}F_{12}FeN_{11}O_2P_2$ C, 38.22; H, 3.43; N, 16.91. Found: C 38,07, H 3,42, N 16,88.

NMR spectra

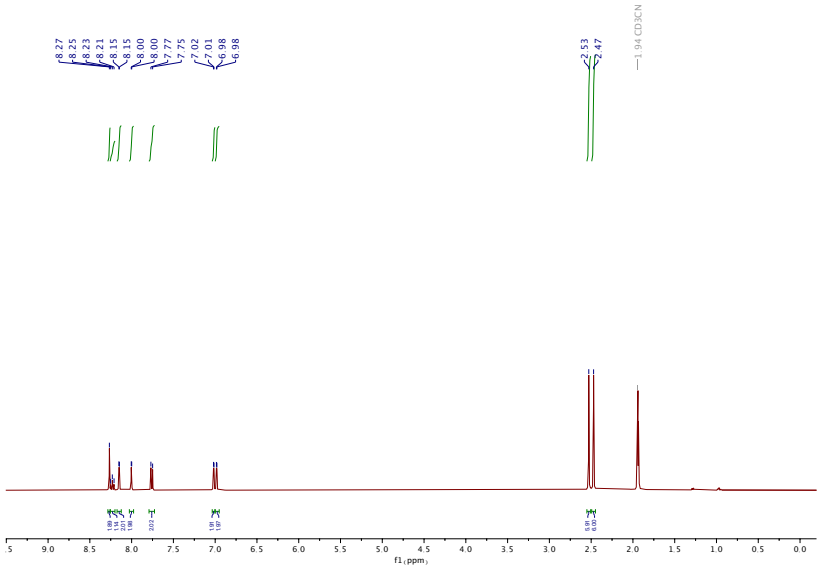

Figure S1: ^{1}H NMR (CD_3CN) spectrum of ((1,1'-(4-Carboxypyridine-2,6-diyl)bis(3-methylimidazol-2-ylidene))(1,1'-(pyridine-2,6-diyl)bis(3-methylimidazol-2-ylidene))iron(II)) bis(hexafluorophosphate) ([Fe(cpbmi)(pbmi)]$(PF_6)_2$ (**1**)).

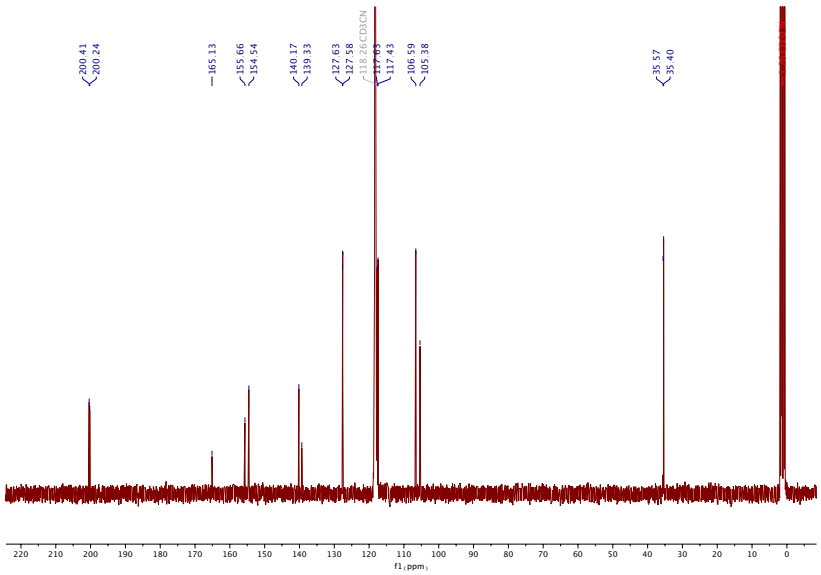

Figure S2: ^{13}C NMR (CD_3CN) spectrum of ((1,1'-(4-Carboxypyridine-2,6-diyl)bis(3-methylimidazol-2-ylidene))(1,1'-(pyridine-2,6-diyl)bis(3-methylimidazol-2-ylidene))iron(II)) bis(hexafluorophosphate) ([Fe(cpbmi)(pbmi)]$(PF_6)_2$ (**1**)).

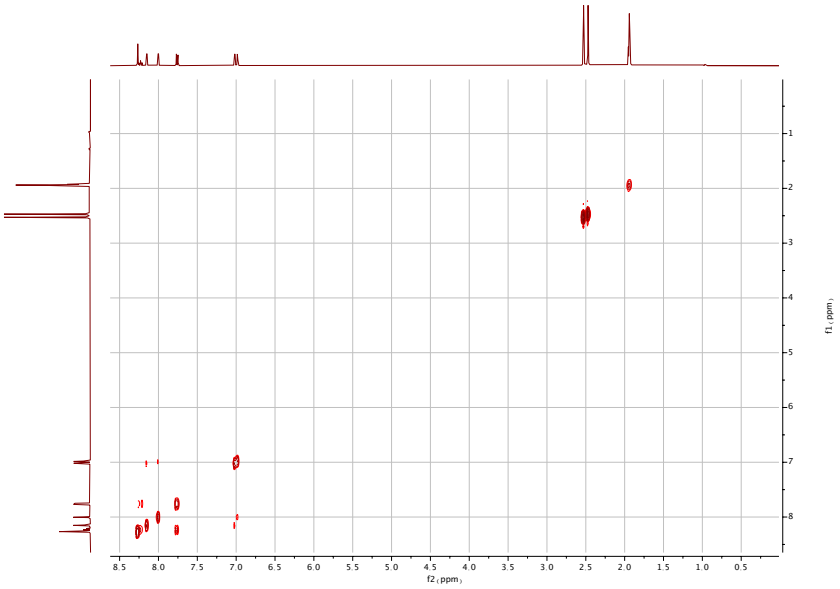

Figure S3: COSY NMR (CD_3CN) spectrum of ((1,1'-(4-Carboxypyridine-2,6-diyl)bis(3-methylimidazol-2-ylidene))(1,1'-(pyridine-2,6-diyl)bis(3-methylimidazol-2-ylidene))iron(II)) bis(hexafluorophosphate) ([Fe(cpbmi)(pbmi)]$(PF_6)_2$ (**1**)).

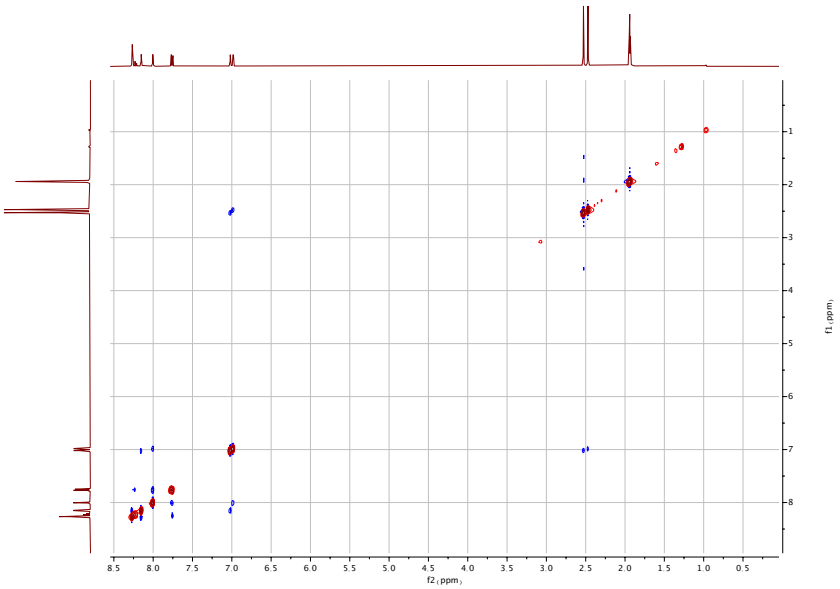

Figure S4: NOESY NMR (CD_3CN) spectrum of ((1,1'-(4-Carboxypyridine-2,6-diyl)bis(3-methylimidazol-2-ylidene))(1,1'-(pyridine-2,6-diyl)bis(3-methylimidazol-2-ylidene))iron(II)) bis(hexafluorophosphate) ([Fe(cpbmi)(pbmi)]$(PF_6)_2$ (**1**)).

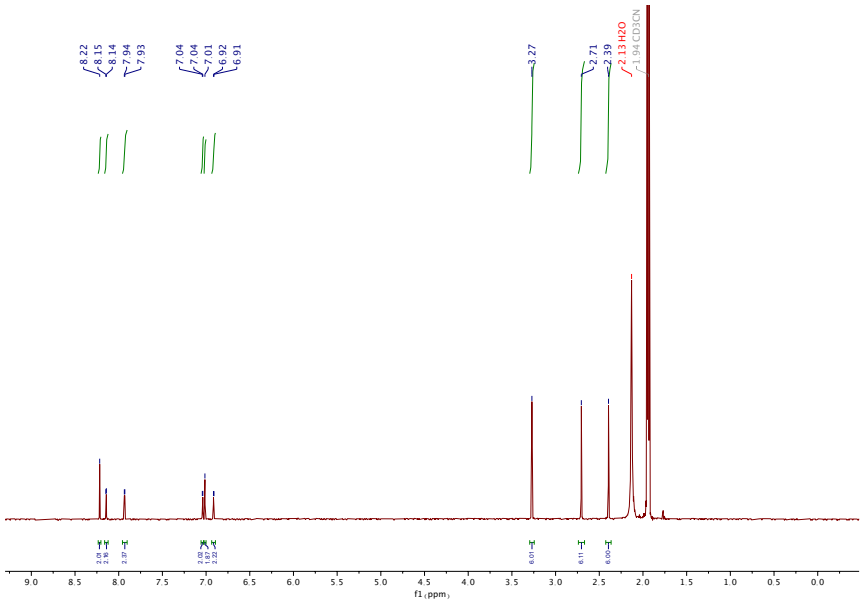

Figure S5: ^{1}H NMR (CD_3CN) spectrum of (1,1'-(4-carboxypyridine-2,6-diyl)bis(3-methylimidazol-2-ylidene))(1,1'-(4-(Dimethylamino)pyridine-2,6-diyl)bis(3-methylimidazol-2-ylidene))iron(II) bis(hexafluorophosphate) ([Fe(cpbmi)(dmapbmi)]$(PF_6)_2$ (**4**)).

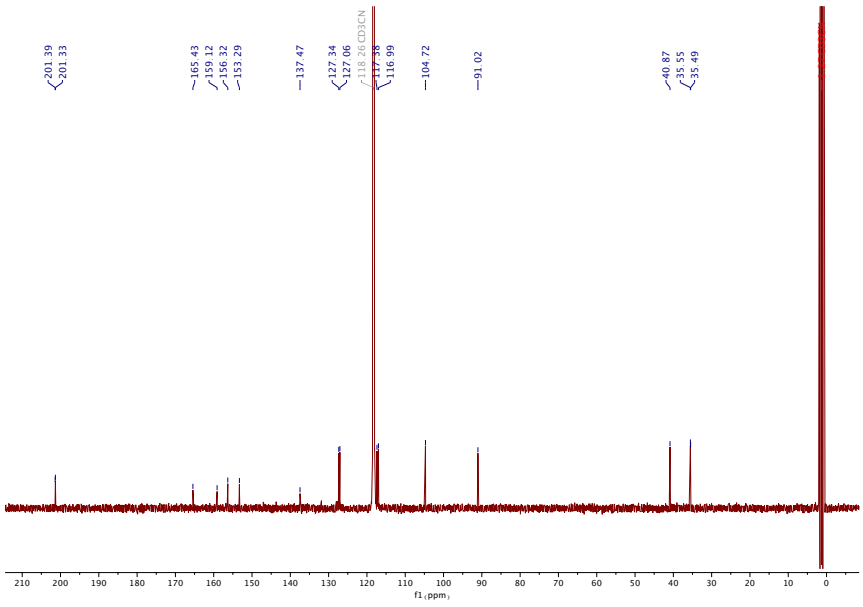

Figure S6: ^{13}C NMR (CD_3CN) spectrum of (1,1'-(4-carboxypyridine-2,6-diyl)bis(3-methylimidazol-2-ylidene))(1,1'-(4-(Dimethylamino)pyridine-2,6-diyl)bis(3-methylimidazol-2-ylidene))iron(II) bis(hexafluorophosphate) ([Fe(cpbmi)(dmapbmi)]$(PF_6)_2$ (**4**)).

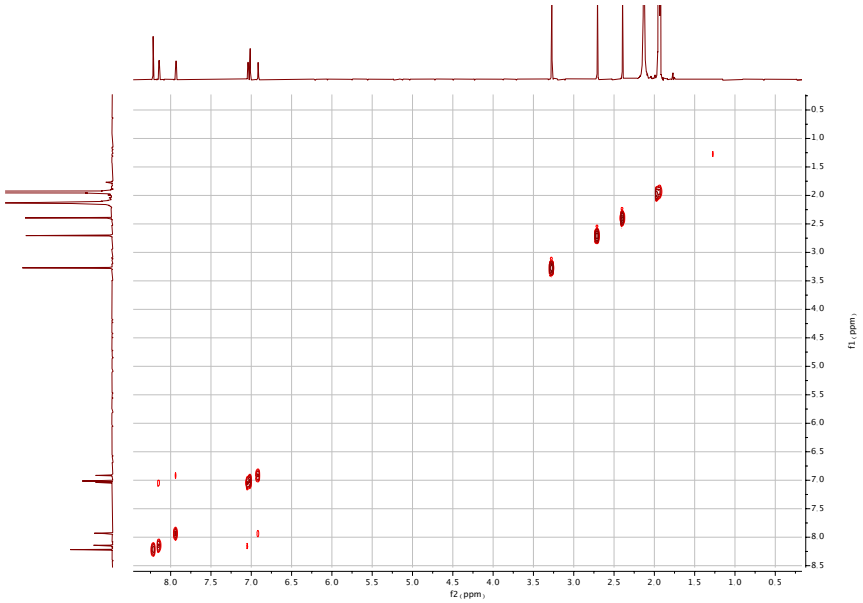

Figure S7: COSY NMR (CD_3CN) spectrum of (1,1'-(4-carboxypyridine-2,6-diyl)bis(3-methylimidazol-2-ylidene))(1,1'-(4-(Dimethylamino)pyridine-2,6-diyl)bis(3-methylimidazol-2-ylidene))iron(II) bis(hexafluorophosphate) ([Fe(cpbmi)(dmapbmi)]$(PF_6)_2$ (**4**)).

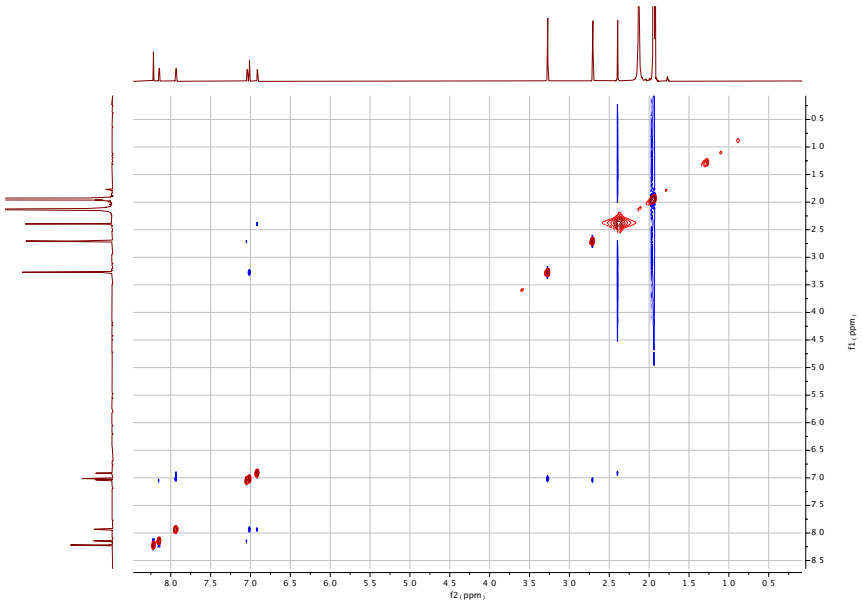

Figure S8: NOESY NMR (CD_3CN) spectrum of (1,1'-(4-carboxypyridine-2,6-diyl)bis(3-methylimidazol-2-ylidene))(1,1'-(4-(Dimethylamino)pyridine-2,6-diyl)bis(3-methylimidazol-2-ylidene))iron(II) bis(hexafluorophosphate) ([Fe(cpbmi)(dmapbmi)]$(PF_6)_2$ (**4**)).

Steady state absorption

Steady-state absorption measurements in the UV-VIS region were performed in an Agilent Technologies Cary 60 UV-Vis Spectrophotometer. For each complex, careful dilution series were carried out in acidic solution ensuring constant ionic strength (0.1 M TBA methanesulfonate and 0.1 M methanesulfonic acid in acetonitrile). All acetonitrile was collected from dry solvent dispenser (Innovative technology, PS-micro) and stored over 3 Å MS. The complexes were weighting to an accuracy of ~2 µg, then dissolved in the respective solvent system to a known concentration using volumetric flasks. All dilutions were diluted by a factor of 2 compared to the next more concentrated solution, using volumetric pipettes and volumetric flasks. For all dilution series a minimum of 5 different

concentrations spanning at least one order of magnitude were used. Absorbance of all prepared concentrations was, after filtration through a syringe filter (Fisherbrand, PTFE, 0.45 µm porosity, 13 mm diameter), measured in a standard quartz-glass cuvette of path length 1 cm (HellmaAnalytics – High Precision Quartz Glass). For reference the same cuvette with solution used to dissolve the complexes (0.1 M TBA methanesulfonate and 0.1 M methanesulfonic acid in acetonitrile), was used for each dilution series. Extinction coefficients were evaluated where appropriate by performing a linear fit to the absorbance as a function of concentration for each wavelength, after the reference measurement had been subtracted.

Fabrication of solar cell devices

On cleaned (Hellmanex III solution, water, ethanol, UV-ozone) Nippon sheet glass (Pilkington, St. Helens, UK), 8 Ω sheet resistance, a dense TiO_2 layer was deposited via spray pyrolysis at 450 °C from a 0.6M titanium diisopropoxide bis(acetylacetonate)solution in isopropanol. Subsequently, 7 mm diameter TiO_2 photoanodes were screen-printed (Seritec Services SA, Corseaux, Switzerland) from DSL 18 NR-T (GreatCellSolar, Queanbeyan, Australia) colloidal (18 nm) TiO_2 paste (32 µm). The full mesoporous layer thickness was screen-printed as 6 consecutive layers, with an annealing step at 450 °C between each deposited layer. Subsequently, the final layer was heated to 125 °C and a scattering layer (GreatCellSolar WER2-O, 400 nm) was screen-printed onto of the mesoporous film (4 µm), followed by gradual heating towards a 30 min sintering step at 450 °C. The substrates were post-treated with a 40 mM aqueous $TiCl_4$ solution for 30 min at 70 °C and then again followed by gradual heating towards a 30 min sintering step at 450 °C. After cooling, the titania films were immersed sequentially into two different solutions, each overnight. The first solution contained 0.2 mM (for dye **1**) or 0.05 mM (for dye **2**, **3** and **4**) of each sensitizer in acetonitrile, while the second contained 0.5 mM chenodeoxycholic acid in acetonitrile, as has been suggested in literature.[S3] Platinized counter electrodes were fabricated through drop casting twice 20 µL of a 5 mM solution of $H_2PtCl_6 \cdot 6\ H_2O$ in ethanol onto predrilled TEC7 glass followed by 30 minutes of sintering at 400 °C.[S5] The redox electrolyte solution contained 0.1 M LiI, 0.05 M I_2 and 0.6M 1-methyl-3-propylimidazolium iodide in 3-methoxypropionitrile as proposed in reference.[S6] The cells were assembled using UV curing sealant (ThreeBond, Milton Keynes, United Kingdom/International). The electrolyte was injected through a hole in the counter electrode (approx. 1 mm Ø), the outlet was sealed with UV curing sealant and the hole in the counter electrode was then sealed with a thermoplastic surlyn film (Meltonix, Solaronix, Switzerland) and a glass cover slip.

Characterization of solar cell devices

Current-Voltage measurements

Current-Voltage measurements were carried out in ambient air under AM 1.5G illumination using a Sinus-70 solar simulator (Wavelabs Solar Metrology Systems GmbH, Leipzig, Germany). An X2000 source meter (Ossila, Sheffield, UK) was used to assess solar cell performance (50 mV s^{-1}). A mask was employed to confine the active solar cell area to 0.196 cm^2. The scan rate was measuremed to 38 mV/s.

Table S1: Comparison of average characteristics from DSC devices from a single batch, assembled using thermoplastic surlyn or UV-curing glue.

Dye, assembly method	V_{OC} (V)	J_{SC} (mA cm^{-2})	FF	PCE (%)
Dye 1, Surlyn	0.535	1.14	0.702	0.43
Dye 1, UV-Glue	0.519	1.62	0.644	0.54
Dye 2, Surlyn	0.509	1.52	0.722	0.56
Dye 2, UV-Glue	0.492	2.66	0.666	0.87
Dye 3, Surlyn	0.477	0.76	0.746	0.27
Dye 3, UV-Glue	0.449	1.68	0.680	0.51

Table S2: Comparison of average characteristics from DSC devices from a single batch, assembled using sensitization baths of 0.05 M and 0.2 M of the dyes.

Dye, sensitization bath conc.	V_{OC} (V)	J_{SC} (mA cm^{-2})	FF	PCE (%)
Dye 1, 0.05 M	0.483	2.21	0.643	0.68
Dye 1, 0.2 M	0.466	3.39	0.621	0.98
Dye 2, 0.05 M	0.485	3.44	0.635	1.06
Dye 2, 0.2 M	0.404	2.66	0.675	0.72
Dye 3, 0.05 M	0.455	3.36	0.625	0.96
Dye 3, 0.2 M	0.339	1.89	0.666	0.43
Dye 4, 0.05 M	0.474	3.97	0.626	1.18
Dye 4, 0.2 M	0.409	3.63	0.674	1.00

Table S3: Comparison of average characteristics from DSC devices from a single batch, assembled using electrolyte of 0.1 M LiI, 0.1 M I_2 and 0.6 M MPII in MPN (ele 1) and a saturated solution of the mixture of 0.1 M LiI, 0.1 M I_2, 0.1 M MgI_2, 0.1 M Gunidinium thiocyanate, 0.1 M tetrabutylammonium iodide and 0.6 M MPII in MPN (ele 2).

Dye, electrolyte	V_{OC} (V)	J_{SC} (mA cm^{-2})	FF	PCE (%)
Dye 1, ele 1	0.497	3.12	0.602	0.93
Dye 1, ele 2	0.431	4.48	0.566	1.09
Dye 2, ele 1	0.475	3.52	0.625	1.04
Dye 2, ele 2	0.414	4.12	0.591	1.01
Dye 4, ele 1	0.462	4.39	0.537	1.28
Dye 4, ele 2	0.434	5.14	0.559	1.25

Table S4: Comparison of average characteristics from DSC devices from a single batch, assembled using a saturated solution of the mixture of 0.1 M LiI, 0.1 M I_2, 0.1 M MgI_2, 0.1 M Gunidinium thiocyanate, 0.1 M tetrabutylammonium iodide and 0.6 M MPII in MPN (ele 2), and electrolyte of 0.1 M LiI, 0.1 M I_2, 0.1 M MgI_2, 0.1 M Gunidinium thiocyanate, 0.1 M tetrabutylammonium iodide and 0.6 M MPII in MeCN (ele 3)

Dye, electrolyte	V_{OC} (V)	J_{SC} (mA cm^{-2})	FF	PCE (%)
Dye 2, ele 2	0.411	4.86	0.558	1.12
Dye 2, ele 3	0.393	2.65	0.554	0.65
Dye 3, ele 2	0.416	3.32	0.625	0.86
Dye 3, ele 3	0.334	2.59	0.623	0.54
Dye 4, ele 2	0.453	4.59	0.615	1.28
Dye 4, ele 3	0.396	4.28	0.612	1.04

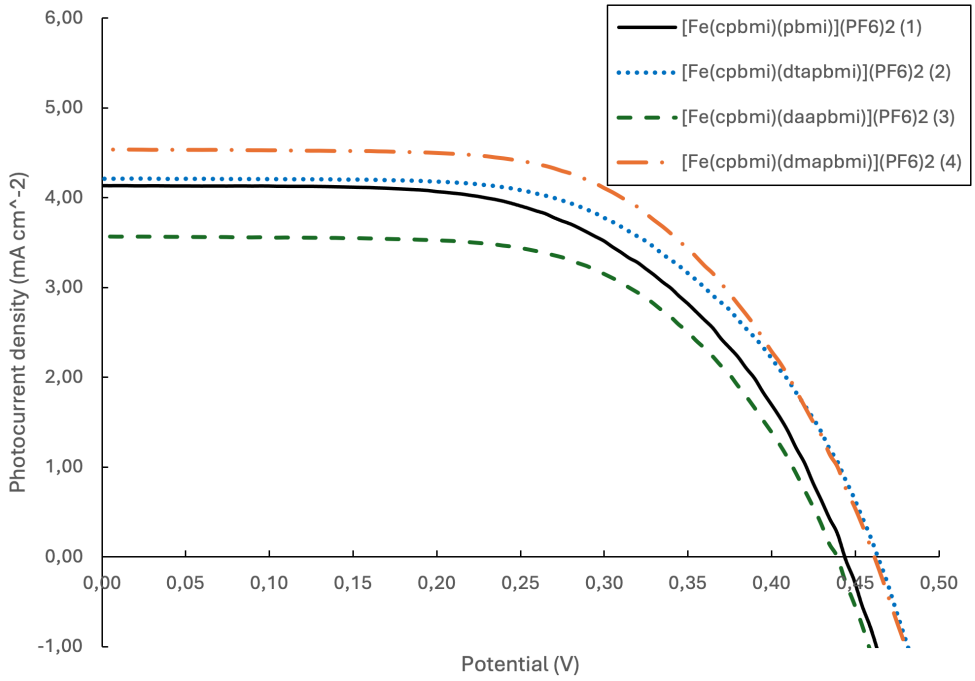

Figure S9: Measured *J-V* characteristics at AM 1.5G illumination for best performing solar cells (with regards to PCE) sensitized with dyes 1-4, on 18 nm particle TiO_2, scanning from SC to OC.

Table S5: Solar cell characteristics for best performing cells (with regards to PCE) sensitized with dyes 1-4, on 18 nm particle TiO_2, scanning from SC to OC. Open-circuit voltage (V_{OC}), short-circuit current density (J_{SC}), fill-factor (FF) and power conversion efficiency (PCE). Average of six cells from the same batch, with standard deviation of all measurements, within parentheses.

Dye	V_{OC} (mV)	J_{SC} (mA cm^{-2})	$J_{SC,\ IPCE}$ (mA cm^{-2})	FF	PCE (%)
[Fe(cpbmi)(pbmi)](PF$_6$)$_2$ (**1**)	443 (448±1)	4.13 (3.85±0.07)	4.15	0.575 (0.589±0.001)	1.05 (1.02±0.01)
[Fe(cpbmi)(dtapbmi)](PF$_6$)$_2$ (**2**)	463 (461±1)	4.21 (3.94±0.02)	3.38	0.586 (0.590±0.001)	1.14 (1.069±0.007)
[Fe(cpbmi)(daapbmi)](PF$_6$)$_2$ (**3**)	439 (438±1)	3.57 (3.38±0.07)	3.40	0.605 (0.609±0.001)	0.95 (0.90±0.01)
[Fe(cpbmi)(dmapbmi)](PF$_6$)$_2$ (**4**)	461 (469±0.4)	4.54 (4.26±0.03)	4.66	0.596 (0.608±0.001)	1.25 (1.211±0.002)

IPCE measurements

IPCE spectra were recorded with a PVE300 photovoltaic QE system (Bentham, Reading, United Kingdom) and a TMc300 monochromator (Bentham, Reading, United Kingdom).

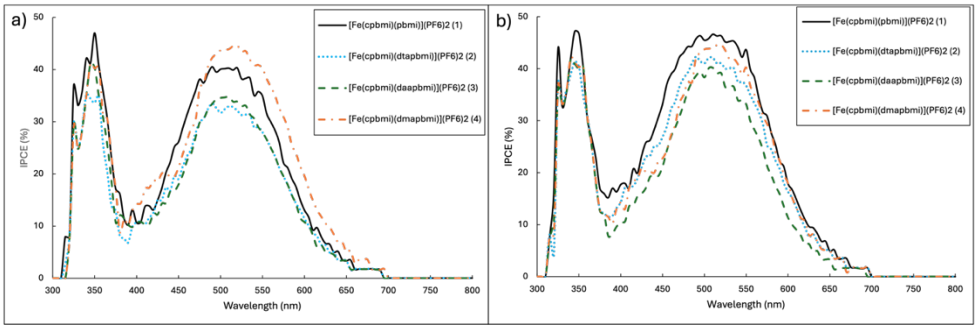

Figure S10: IPCE spectra for best performing solar cells (with regards to PCE) sensitized with dyes 1-4. a) shows devices made with substrates with 18 nm TiO_2 particles, and b) shows devices made with substrates with a 1:1 mixture of 18 nm and 30 nm TiO_2 particles.

Electron recombination lifetimes

Electron recombination lifetimes were investigated using the DSC *Toolbox* (Dyenamo, Stockholm, Sweden). The solar cell was illuminated with a 1 W white LED. Kinetics in the solar cell were probed by applying square-wave modulations to the light intensity. The solar cell voltage response was tracked by a digital acquisition board and fitted with first-order kinetic models.

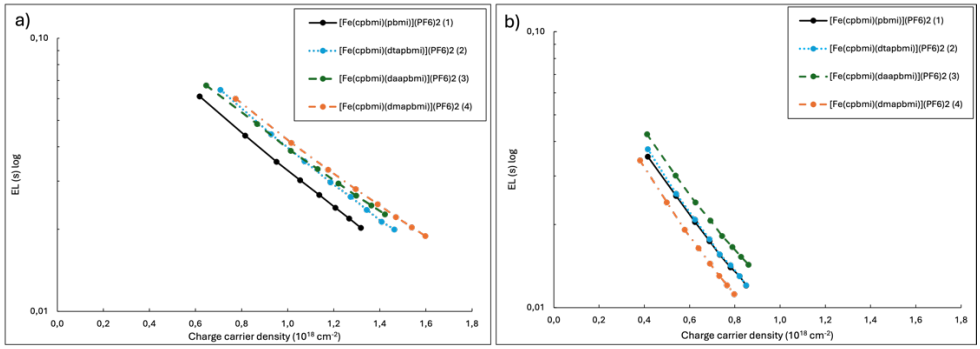

Figure S11: Electron lifetimes plotted against charge carrier density for best performing solar cells (with regards to PCE) sensitized with dyes 1-4. a) shows devices made with substrates with 18 nm TiO_2 particles, and b) shows devices made with substrates with a 1:1 mixture of 18 nm and 30 nm TiO_2 particles.

Comparative scans from OC to SC

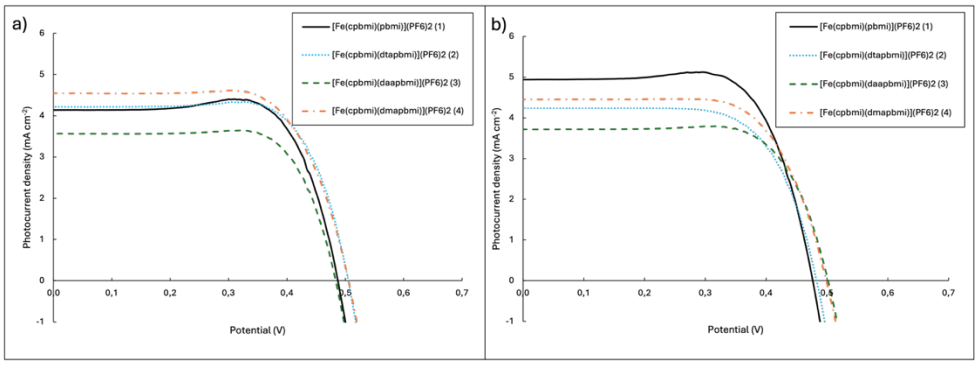

Figure S12: Measured *J-V* characteristics at AM 1.5G illumination for best performing solar cells (with regards to PCE) sensitized with dyes 1-4, scanning from OC to SC. a) shows devices made with substrates with 18 nm TiO_2 particles, and b) shows devices made with substrates with a 1:1 mixture of 18 nm and 30 nm TiO_2 particles.

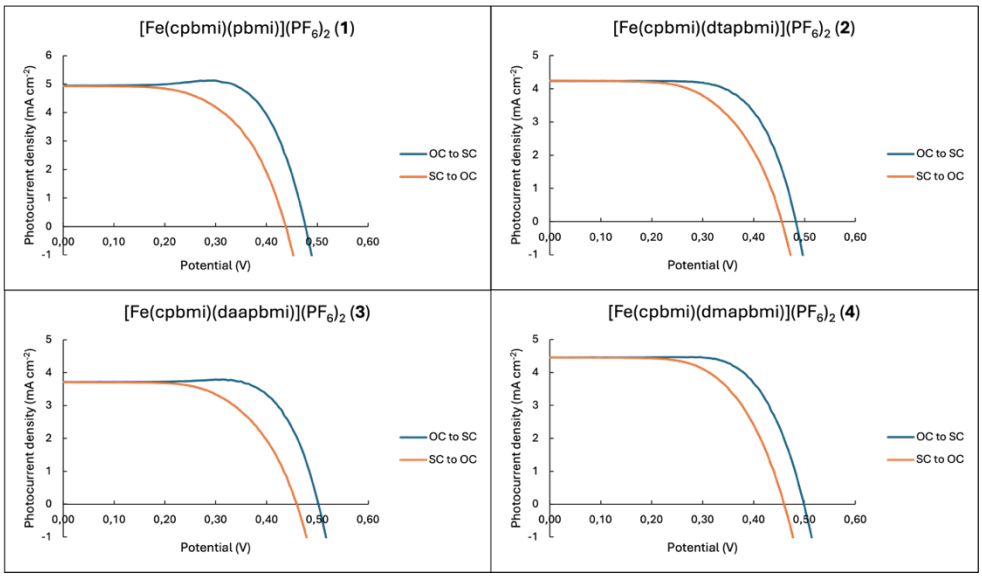

Figure S13: Comparison of *J-V* scans for each investigated dye, scanning from OC to SC, and scanning from SC to OC

Table S6: Solar cell characteristics for best performing cells (with regards to PCE) sensitized with dyes 1-4, on 18 nm particle TiO_2, scanning from OC to SC. Open-circuit voltage (V_{OC}), short-circuit current density (J_{SC}), fill-factor (FF), power conversion efficiency (PCE) and hysteresis index. Average of six cells from the same batch, with standard deviation within parentheses.

Dye	V_{OC} (mV)	J_{SC} (mA cm^{-2})	FF	PCE (%)	Hysteresis index
[Fe(cpbmi)(pbmi)](PF$_6$)$_2$ (**1**)	496 (492±1)	3,93 (3.84±0.06)	0,811 (0.810±0.002)	1,58 (1.53±0.01)	0.214 (0.202±0.003)
[Fe(cpbmi)(dtapbmi)](PF$_6$)$_2$ (**2**)	500 (502±1)	4.22 (3.94±0.02)	0.732 (0.751±0.002)	1.55 (1.48±0.01)	0.151 (0.163±0.007)
[Fe(cpbmi)(daapbmi)](PF$_6$)$_2$ (**3**)	484 (484±2)	3.57 (3.38±0.07)	0.744 (0.735±0.003)	1.29 (1.20±0.04)	0.151 (0.14±0.01)
[Fe(cpbmi)(dmapbmi)](PF$_6$)$_2$ (**4**)	505 (511±0.5)	4.54 (4.26±0.03)	0.700 (0.723±0.001)	1.61 (1.573±0.002)	0.127 (0.130±0.001)

Table S7: Solar cell characteristics for best performing cells (with regards to PCE) sensitized with dyes 1-4, on 18 nm and 30 nm particle TiO_2, scanning from OC to SC. Open-circuit voltage (V_{OC}), short-circuit current density (J_{SC}), fill-factor (FF), power conversion efficiency (PCE) and hysteresis index. Average of six cells from the same batch, with standard deviation within parentheses.

Dye	V_{OC} (mV)	J_{SC} (mA cm^{-2})	FF	PCE (%)	Hysteresis index
[Fe(cpbmi)(pbmi)](PF$_6$)$_2$ (**1**)	476 (480±1)	4.91 (4.2±0.3)	0.729 (0.744±0.004)	1.70 (1.51±0.05)	0,150 (0,158±0.002)
[Fe(cpbmi)(dtapbmi)](PF$_6$)$_2$ (**2**)	513 (486±2)	3.96 (4.08±0.06)	0.718 (0.704±0.001)	1.46 (1.40±0.02)	0,107 (0,11±0.02)
[Fe(cpbmi)(daapbmi)](PF$_6$)$_2$ (**3**)	502 (497±4)	3.72 (3.4±0.2)	0.723 (0.717±0.008)	1.35 (1.19±0.06)	0,141 (0,12±0.02)
[Fe(cpbmi)(dmapbmi)](PF$_6$)$_2$ (**4**)	522 (511±2)	4.19 (4.21±0.08)	0.698 (0.697±0.001)	1.53 (1.493±0.005)	0,106 (0,104±0.001)

Maintained voltage measurements

Stable voltage measurements were carried out on same equipment as *J-V* measurements. The difference in voltage corelates to the magnitude of hysteresis for the different dyes.

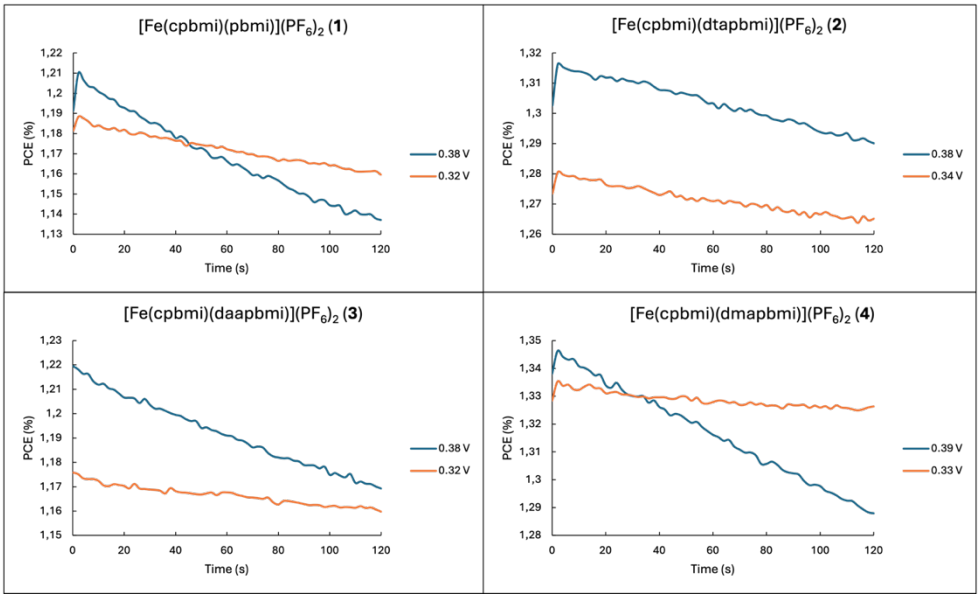

Figure S14: Current density over time under constant voltage, for DSC-devices based on dyes 1-4, on TiO_2 of 18 nm particle size.

10% sunlight measurements

J-V measurements under low light conditions were carried out under conditions as used for full sun light measurements, but with lower simulates sun intensity.

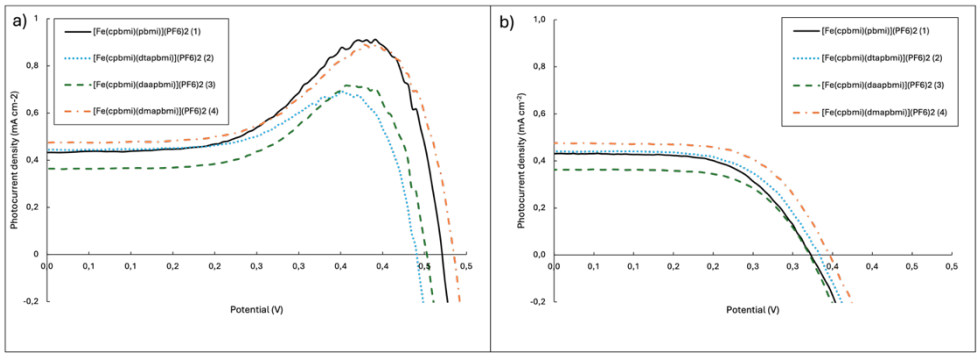

Figure S15: Measured *J-V* characteristics at 10% AM 1.5G illumination for best performing solar cells (with regards to PCE) sensitized with dyes 1-4, sensitized on substrates with 18 nm TiO_2 particles. a) Scanning from OC to SC, and b) scanning from SC to OC.

Table S8: Solar cell characteristics for best performing cells (with regards to PCE) sensitized with dyes 1-4, on 18 nm particle TiO_2, measured under 10% simulated sunlight, scanning from SC to OC. Open-circuit voltage (V_{OC}), short-circuit current density (J_{SC}), fill-factor (FF) and power conversion efficiency (PCE).

Dye	V_{OC} (V)	J_{SC} (mA cm^{-2})	FF	PCE (%)
[Fe(cpbmi)(pbmi)]$(PF_6)_2$ (**1**)	0.321	0.43	0.602	0.83
[Fe(cpbmi)(dtapbmi)]$(PF_6)_2$ (**2**)	0.33	0.44	0.602	0.87
[Fe(cpbmi)(daapbmi)]$(PF_6)_2$ (**3**)	0.32	0.36	0.629	0.73
[Fe(cpbmi)(dmapbmi)]$(PF_6)_2$ (**4**)	0.345	0.48	0.621	1.02

References

S1. Harlang, T. C.; Liu, Y.; Gordivska, O.; Fredin, L. A.; Ponseca, C. S.; Huang, P.; Chábera, P.; Kjaer, K. S.; Mateos, H.; Uhlig, J.; Lomoth, R.; Wallenberg, R.; Styring, S.; Persson, P.; Sundström, V.; Wärnmark, K., Iron sensitizer converts light to electrons with 92% yield. *Nat. Chem.* **2015,** *7* (11), 883-889.

S2. Vukadinovic, Y.; Burkhardt, L.; Päpcke, A.; Miletic, A.; Fritsch, L.; Altenburger, B. r.; Schoch, R.; Neuba, A.; Lochbrunner, S.; Bauer, M., When donors turn into acceptors: Ground and excited state properties of FeII complexes with amine-substituted tridentate bis-imidazole-2-ylidene pyridine ligands. *Inorg. Chem.* **2020,** *59* (13), 8762-8774.

S3. Lindh, L.; Gordivska, O.; Persson, S.; Michaels, H.; Fan, H.; Chábera, P.; Rosemann, N. W.; Gupta, A. K.; Benesperi, I.; Uhlig, J.; Prakash, O.; Sheibani, E.; Kjaer, K. S.; Boschloo, G.; Yartsev, A.; Freitag, M.; Lomoth, R.; Persson, P.; Wärnmark, K., Dye-sensitized solar cells based on Fe N-heterocyclic carbene photosensitizers with improved rod-like push-pull functionality. *Chemical science* **2021,** *12* (48), 16035-16053.

S4. Weast, R. C., *CRC handbook of chemistry and physics Sixty-seventh edition*. CRC Press Inc: United States, 1986.

S5. Feldt, S. M.; Gibson, E. A.; Wang, G.; Fabregat, G.; Boschloo, G.; Hagfeldt, A., Carbon counter electrodes efficient catalysts for the reduction of Co (III) in cobalt mediated dye-sensitized solar cells. *Polyhedron* **2014,** *82*, 154-157.

S6. Karpacheva, M.; Housecroft, C. E.; Constable, E. C., Electrolyte tuning in dye-sensitized solar cells with N-heterocyclic carbene (NHC) iron(II) sensitizers. *Beilstein J. Nanotechnol.* **2018,** *9*, 3069-3078.